

The origin of the Fe K features in Markarian 205 and Markarian 509

M.J. Page¹, S.W. Davis², N.J. Salvi¹

¹*Mullard Space Science Laboratory, University College London, Holmbury St Mary, Dorking, Surrey, RH5 6NT, UK*

²*Department of Physics, University of California, Santa Barbara, CA 93106, USA*

29 October 2018

ABSTRACT

We examine the 3–10 keV EPIC spectra of Mrk 205 and Mrk 509 to investigate their Fe K features. The most significant feature in the spectra of both objects is an emission line at 6.4 keV. The spectra can be adequately modelled with a power law and a relatively narrow ($\sigma < 0.2$ keV) Fe K α emission line. Better fits are obtained when an additional Gaussian emission line, relativistic accretion-disk line, or Compton reflection from cold material, is added to the spectral model. We obtain similar goodness of fit for any of these three models, but the model including Compton reflection from cold material offers the simplest, physically self-consistent solution, because it only requires one reprocessing region. Thus the Fe K spectral features in Mrk 205 and Mrk 509 do not present strong evidence for reprocessing in the inner, relativistic parts of accretion disks.

Key words: accretion, accretion disks – black hole physics – galaxies: Seyfert –

1 INTRODUCTION

X-ray observations probe the central regions of AGN. In the standard paradigm, this corresponds to the inner parts of an accretion disk around a supermassive black hole. Above the disk, a hot corona Compton upscatters optical-EUV photons to X-ray energies; some of this X-ray radiation is reprocessed in the surrounding material including the disk, giving rise to prominent Fe K α lines. The broad, distorted velocity profile of Fe K α emission, suggesting an accretion disk around a supermassive black hole, was first observed with *ASCA* in MCG –6-30-16 (Tanaka et al. 1995). This profile, with a sharp blue wing and a broad red tail, is a remarkable probe of the strong gravity regime.

Studies of other AGN with *ASCA* suggested that broad, low-ionisation Fe K α emission is common in AGN (Nandra et al. 1997, Reynolds et al. 1997), but it was not until the launch of *XMM-Newton* that the diversity of Fe line profiles could really be investigated. With the large increase in collecting area afforded by *XMM-Newton*, it was soon noticed that some luminous AGN showed different Fe line profiles to that of MCG –6-30-15 (e.g. Reeves et al. 2001a, Blustin et al. 2002). One particularly interesting example, the luminous Seyfert 1 galaxy Mrk 205, appeared to have a narrow, neutral Fe K α line at 6.4 keV, accompanied by a broad line from He-like Fe (Reeves et al. 2001b). Reeves et al. argued that the ionised Fe line originates in the inner parts of an accretion disk, while

the neutral Fe K α line originates in a molecular torus, hypothesised to lie outside the broad line regions in AGN unification schemes (Antonucci 1993). A later observation of another Seyfert galaxy, Mrk 509, showed a very similar pair of narrow-neutral and broad-ionised Fe K α emission lines (Pounds et al. 2001), demonstrating that this configuration of Fe K α profiles is not an isolated phenomenon in Mrk 205.

In this paper we revisit the Fe K features in Mrk 205 and Mrk 509 seen by *XMM-Newton*. By coadding the spectra from the three EPIC instruments we are able to maximise the signal to noise per bin while properly sampling the EPIC spectral resolution around Fe K. The paper is laid out as follows. In Section 2 we describe the observations and data reduction, and we describe the spectral fitting in Section 3. The results are discussed in Section 4 and we present our conclusions in Section 5. The Appendix contains a description of the method employed to coadd spectra from the different EPIC instruments.

2 OBSERVATIONS AND DATA REDUCTION

Mrk 205 was observed with *XMM-Newton* on the 7th May 2000, and these data were presented by Reeves et al. (2001b). Several exposures were taken in both MOS and PN cameras, in full frame and large-window modes. Spectra of the source were extracted from circular regions of radius $\sim 50''$ and background spectra were obtained

Table 1. *XMM-Newton* observations of Mrk 205 and Mrk 509

Object	Date	Exposure (ks)	Count rate (count s ⁻¹)
Mrk 205	7 May 2000	49.0	4.9
Mrk 509	25 November 2000	23.4	26.7
Mrk 509	20 April 2001	30.6	38.3

from nearby source-free regions. All valid event patterns (singles, doubles, and triples) were selected in MOS, and only single events in PN. The spectra were combined using the procedure outlined in Appendix A.

Mrk 509 has been observed twice with *XMM-Newton*. The first observation took place on 25th November 2000 and the data were presented by Pounds et al. (2001). The second observation was performed on the 20th April 2001. In both observations, MOS and PN cameras were operated in small window mode. Source spectra were taken from a circular region of 40'' – 50'' radius, and background spectra were obtained from nearby regions free from bright sources. Single events were selected in MOS, and single and double events were selected in PN. The spectra were combined using the procedure outlined in the Appendix to produce one spectrum for each observation and one spectrum which is a combination of the two.

3 RESULTS

The spectral fitting was performed with XSPEC. Only the rest-frame 3–10 keV energy range was used in the spectral fitting because we are primarily interested in the Fe K features. The broad emission lines reported by Reeves et al. (2001b) and Pounds et al. (2001) are only significant between 5 and 8 keV (see Fig. 4 of Pounds et al. 2001), so the 3–10 keV energy range allows a good measurement of the continuum on either side of Fe K, while excluding the noisier and less-well calibrated data at higher energies and the complex spectrum found at lower energies. We included the small effect of absorption from the Galaxy as a component in all our spectral modelling ($N_H = 2.9 \times 10^{20}$ cm⁻² towards Mrk 205 and $N_H = 4.1 \times 10^{20}$ cm⁻² towards Mrk 509, Dickey & Lockman 1990). The results of the spectral fits are given in Table 2.

3.1 Mrk 205

We began by fitting a power law model. The counts spectrum is shown in Fig. 1, along with the power law model convolved with the instrument response. Like Reeves et al. (2001b) we find this model is a poor fit, and there are significant residuals around 6.4 keV. We therefore added a gaussian emission line, and obtained an acceptable fit, with a resolved line consistent with 6.4 keV Neutral Fe K α . Although the fit was acceptable, residuals remained at ~ 7 keV, and so we tried further fits including one of three additional model components that might plausibly account for these residuals and improve the fit: a gaussian emission line at $E > 6.5$ keV, a relativistically-broadened accretion disk line (Fabian et al. 1989; the “diskline” model in XSPEC), and Compton reflection from cold material

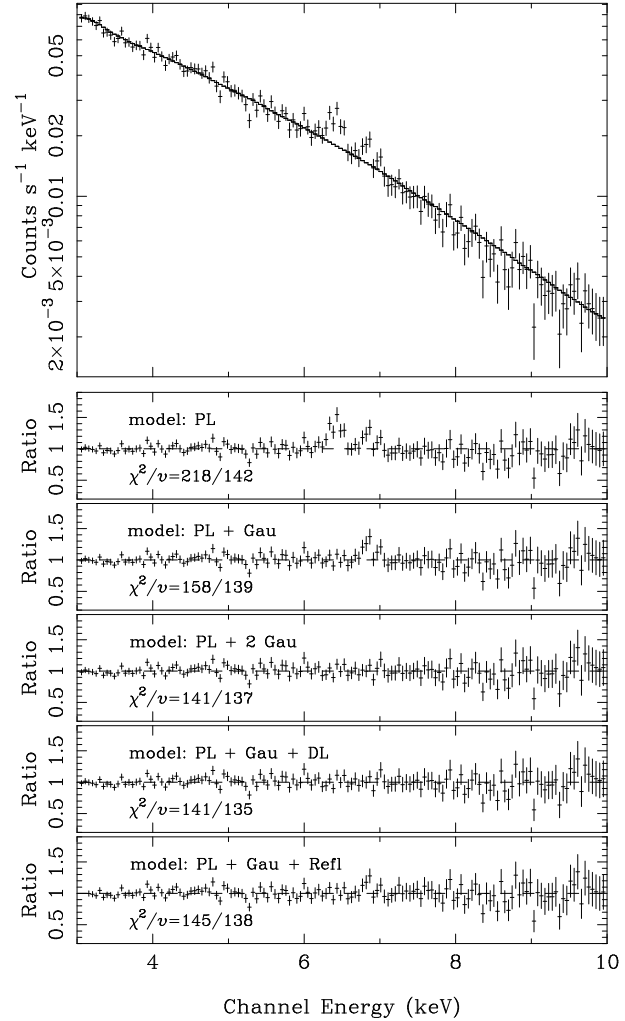


Figure 1. 3–10 keV EPIC spectrum of Mrk 205 and power law model (top panel) and data/model ratio for the five different model fits (lower panels).

(“pexrav” in XSPEC; Magdziarz and Zdziarski 1995). In the diskline model the energy of the line was constrained to lie between 6.7 and 6.9 keV, corresponding to He-like or H-like Fe (as proposed by Reeves et al. 2001b). In the reflection model the inclination was fixed at 45°, and we assumed Solar elemental abundances (Anders and Grevesse 1989). The addition of any of these three components resulted in a similar goodness of fit. The energies of the second Gaussian line and diskline components are found to be consistent with Fe XXVI, and in the case of the diskline the best fit was found for a line produced many R_G from the black hole giving it a narrow profile, similar to that of the Gaussian line. We have also tried more complex models, including two emission lines as well as reflection: the lowest value of $\chi^2/\nu = 138/135$ was obtained when the second emission line is a Gaussian. However, according to the F-test, this is only a 1σ improvement over the model including a single emission line and Compton reflection.

Table 2. Spectral fits. Errors are quoted at 95% confidence for 1 interesting parameter. In cases for which a parameter has reached a limit on the allowed range of values while $\Delta\chi^2 < 4$ the limit has been marked with a '*'. Parameters with values that are fixed in the fit are marked 'F'.

Mrk 205													
Model	Γ	E (keV)	σ (keV)	EW (keV)	E (keV)	σ (keV)	Rin (R_G)	β	i (deg)	EW (keV)	R	χ^2/ν	Prob
PL	1.68 ^{+0.05} _{-0.05}	-	-	-	-	-	-	-	-	-	-	218/142	4.5×10^{-5}
PL+Gau	1.72 ^{+0.05} _{-0.05}	6.42 ^{+0.07} _{-0.04}	0.07 ^{+0.05} _{-0.07*}	0.10 ^{+0.05} _{-0.02}	-	-	-	-	-	-	-	158/139	0.13
PL+2×Gau	1.74 ^{+0.09} _{-0.05}	6.4 ^F	0.07 ^{+0.06} _{-0.04}	0.12 ^{+0.04} _{-0.04}	6.84 ^{+0.08} _{-0.06}	0.04 ^{+0.14} _{-0.04*}	-	-	-	0.06 ^{+0.04} _{-0.03}	-	141/137	0.38
PL+Gau+D.L.	1.74 ^{+0.06} _{-0.05}	6.4 ^F	0.07 ^{+0.05} _{-0.07*}	0.12 ^{+0.04} _{-0.07}	6.88 ^{+0.02*} _{-0.18*}	-	126 ^{+874*} _{-120*}	17 ^{+3*} _{-27*}	0.0 ^{+90.0*} _{-0.0*}	0.06 ^{+0.19} _{-0.03}	-	141/135	0.34
PL+Gau+Refl	1.90 ^{+0.25} _{-0.14}	6.42 ^{+0.03} _{-0.04}	0.04 ^{+0.06} _{-0.04*}	0.08 ^{+0.03} _{-0.03}	-	-	-	-	-	-	2.8 ^{+3.4} _{-1.7}	145/138	0.32
Mrk 509 November 2000													
Model	Γ	E (keV)	σ (keV)	EW (keV)	E (keV)	σ (keV)	Rin (R_G)	β	i (deg)	EW (keV)	R	χ^2/ν	Prob
PL	1.59 ^{+0.03} _{-0.03}	-	-	-	-	-	-	-	-	-	-	302/147	9.6×10^{-13}
PL+Gau	1.62 ^{+0.03} _{-0.03}	6.38 ^{+0.03} _{-0.03}	0.09 ^{+0.05} _{-0.04}	0.09 ^{+0.02} _{-0.02}	-	-	-	-	-	-	-	208/144	3.8×10^{-4}
PL+2×Gau	1.63 ^{+0.03} _{-0.03}	6.4 ^F	0.09 ^{+0.06} _{-0.04}	0.09 ^{+0.02} _{-0.02}	6.98 ^{+0.10} _{-0.38*}	0.11 ^{+0.17} _{-0.11*}	-	-	-	0.03 ^{+0.03} _{-0.02}	-	199/142	1.1×10^{-3}
PL+Gau+DL	1.65 ^{+0.03} _{-0.04}	6.4 ^F	0.06 ^{+0.05} _{-0.06*}	0.07 ^{+0.02} _{-0.02}	6.85 ^{+0.03*} _{-0.15*}	-	6.2 ^{+14.0} _{-0.2*}	-10.0 ^{+6.8} _{-0*}	37 ⁺⁴ ₋₄	0.17 ^{+0.08} _{-0.07}	-	186/140	5.4×10^{-3}
PL+Gau+Refl	1.68 ^{+0.11} _{-0.11}	6.38 ^{+0.04} _{-0.04}	0.07 ^{+0.05} _{-0.05}	0.07 ^{+0.02} _{-0.02}	-	-	-	-	-	-	1.3 ^{+1.3} _{-1.2}	198/143	1.7×10^{-3}
Mrk 509 April 2001													
Model	Γ	E (keV)	σ (keV)	EW (keV)	E (keV)	σ (keV)	Rin (R_G)	β	i (deg)	EW (keV)	R	χ^2/ν	Prob
PL	1.65 ^{+0.03} _{-0.02}	-	-	-	-	-	-	-	-	-	-	226/147	3.0×10^{-5}
PL+Gau	1.68 ^{+0.03} _{-0.03}	6.42 ^{+0.05} _{-0.05}	0.10 ^{+0.08} _{-0.07}	0.07 ^{+0.03} _{-0.02}	-	-	-	-	-	-	-	124/144	0.89
PL+2×Gau	1.69 ^{+0.03} _{-0.03}	6.4 ^F	0.02 ^{+0.09} _{-0.02*}	0.04 ^{+0.04} _{-0.01}	6.60 ^{+0.29} _{-0.00*}	0.27 ^{+0.35} _{-0.27*}	-	-	-	0.05 ^{+0.04} _{-0.04}	-	115/142	0.95
PL+Gau+DL	1.70 ^{+0.03} _{-0.03}	6.4 ^F	0.05 ^{+0.07} _{-0.05*}	0.04 ^{+0.03} _{-0.01}	6.87 ^{+0.03*} _{-0.17*}	-	7.4 ^{+4.0} _{-1.4*}	-4.4 ^{+7.5} _{-5.6*}	27 ⁺⁶ ₋₂₄	0.09 ^{+0.06} _{-0.04}	-	110/140	0.97
PL+Gau+Refl	1.78 ^{+0.07} _{-0.09}	6.41 ^{+0.03} _{-0.03}	0.04 ^{+0.07} _{-0.04*}	0.05 ^{+0.02} _{-0.02}	-	-	-	-	-	-	1.8 ^{+0.9} _{-1.0}	109/143	0.99
Mrk 509 both combined													
Model	Γ	E (keV)	σ (keV)	EW (keV)	E (keV)	σ (keV)	Rin (R_G)	β	i (deg)	EW (keV)	R	χ^2/ν	Prob
PL	1.63 ^{+0.02} _{-0.02}	-	-	-	-	-	-	-	-	-	-	348/147	2.2×10^{-18}
PL+Gau	1.65 ^{+0.02} _{-0.02}	6.40 ^{+0.03} _{-0.03}	0.09 ^{+0.05} _{-0.04}	0.07 ^{+0.02} _{-0.02}	-	-	-	-	-	-	-	161/144	0.16
PL+2×Gau	1.67 ^{+0.03} _{-0.03}	6.4 ^F	0.05 ^{+0.04} _{-0.05*}	0.05 ^{+0.02} _{-0.02}	6.60 ^{+0.41} _{-0.00*}	0.47 ^{+0.42} _{-0.28}	-	-	-	0.07 ^{+0.05} _{-0.05}	-	145/142	0.42
PL+Gau+DL	1.67 ^{+0.03} _{-0.02}	6.4 ^F	0.05 ^{+0.05} _{-0.05*}	0.05 ^{+0.02} _{-0.02}	6.72 ^{+0.18*} _{-0.02*}	-	6.0 ^{+14.5} _{-0.0*}	-3.8 ^{+1.2} _{-6.2*}	34 ⁺⁶ ₋₁₅	0.10 ^{+0.06} _{-0.05}	-	132/140	0.67
PL+Gau+Refl	1.73 ^{+0.06} _{-0.07}	6.40 ^{+0.02} _{-0.03}	0.05 ^{+0.05} _{-0.05*}	0.05 ^{+0.02} _{-0.01}	-	-	-	-	-	-	1.5 ^{+0.8} _{-0.7}	136/143	0.65

Notes:
 PL = power law
 Gau = Gaussian emission line
 DL = accretion disk line (using 'DISKLINE' in XSPEC)
 Refl = Compton reflection component (using 'PEXRAV' in XSPEC)

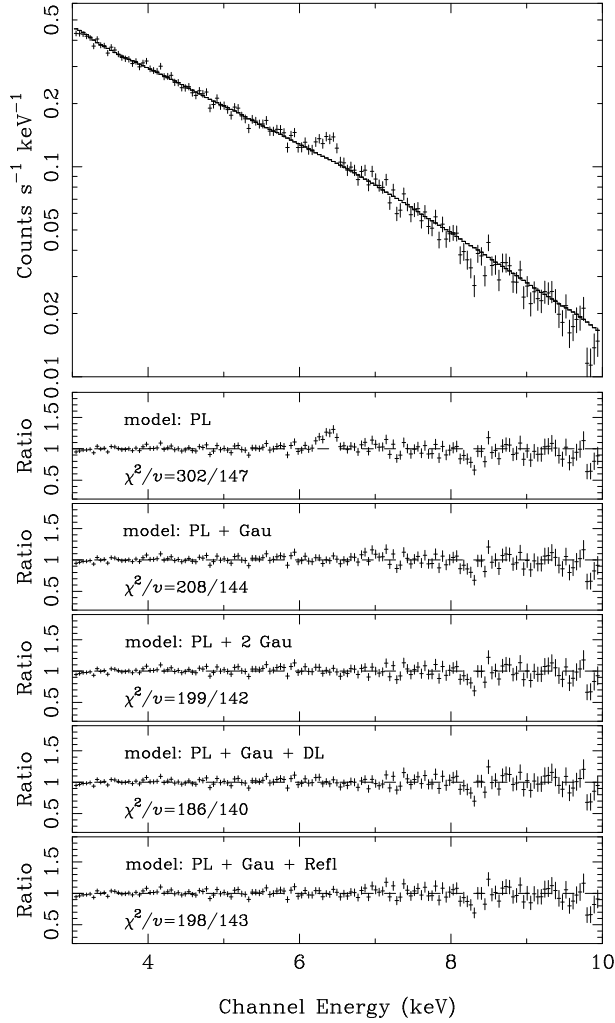


Figure 2. 3-10 keV EPIC spectrum of Mrk 509 from the first observation and power law model (top panel) and data/model ratio for the five different model fits (lower panels).

3.2 Mrk 509 first observation

As for Mrk 205, we began with a power law model and obtained a completely unacceptable fit with large residuals around 6.4 keV (see Fig. 2). Addition of a Gaussian line at ~ 6.4 keV resulted in a much better, but still poor fit (rejected with $> 99.9\%$ confidence). Adding a further Gaussian, a diskline or a reflection component improved the goodness of fit, which is marginally better when the third model component is a diskline rather than a reflection component or a second Gaussian line. However, whichever additional model component is included the model is still unacceptable at $> 99\%$ confidence. We have also tested a more complex model, including a second emission line as well as reflection, and obtain a best $\chi^2/\nu = 182/138$ for a diskline; this is only marginally better (2σ according to the F-test) than the fit with reflection but without the second emission line. Strong residuals at 8.3 and 9.8 keV together contribute ~ 30 to the χ^2 , and are therefore largely responsible for the poor model fit. We have no credible explanation for these residuals other than as statistical fluctuations.

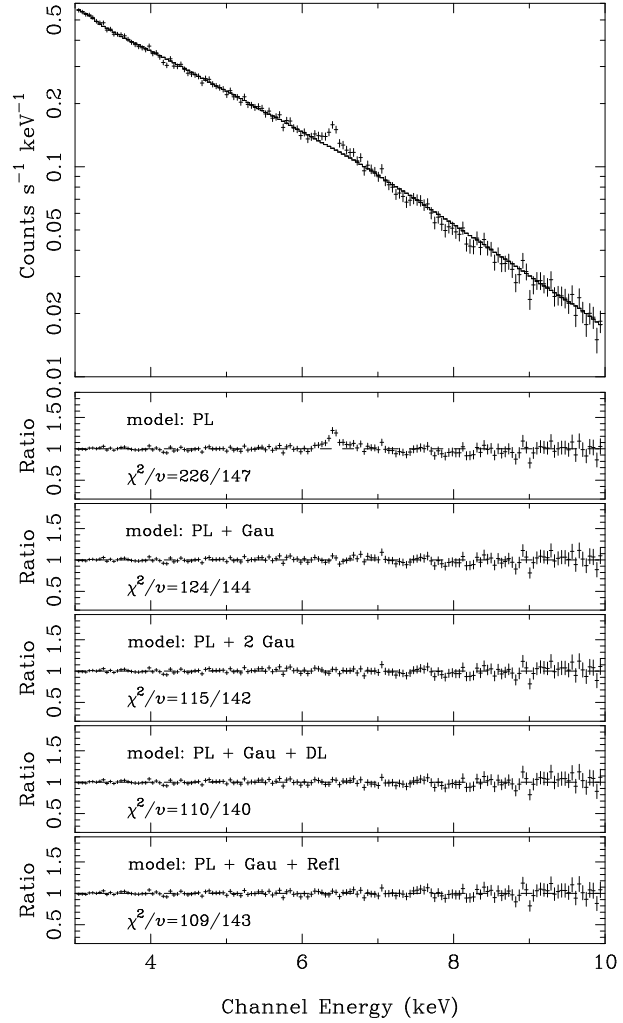


Figure 3. 3-10 keV EPIC spectrum of Mrk 509 from the second observation and power law model (top panel) and data/model ratio for the five different model fits (lower panels).

3.3 Mrk 509 second observation

A power law model provided a poor fit to the spectrum (see Fig. 3), and once again we found that the addition of a ~ 6.4 keV emission line resulted in a significantly improved (and quite acceptable) $\chi^2/\nu=124/144$. The addition of an extra Gaussian, diskline or reflection component each improved the fit further, resulting in very a good fit. However, the addition of a second emission line to the reflection model results in no further improvement in χ^2/ν .

3.4 Mrk 509 both observations combined

The overall spectral shape of Mrk 509 is extremely similar in the two observations, and so to improve signal to noise we have coadded the data from both observations. A model containing only a power law is convincingly rejected, but a power law and a single Gaussian provide an acceptable fit to the data. Adding an additional Gaussian, diskline or reflection component makes a significant improvement to the χ^2/ν (at $> 99.9\%$ significance according to the F-test), resulting in a good fit to the data. Finally,

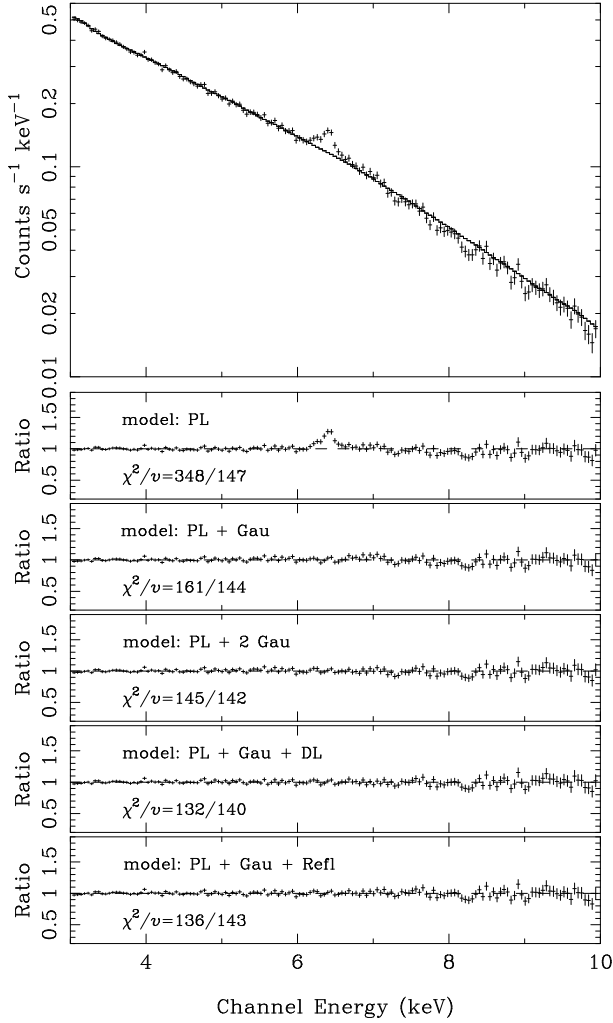


Figure 4. 3-10 keV EPIC spectrum of Mrk 509 (both observations coadded) and power law model (top panel), and data/model ratio for the five different model fits (lower panels).

we have tried more complex models combining reflection with a second Gaussian or accretion-disc emission line. In this case the χ^2/ν is poorer than for the model including reflection without a second emission line.

4 DISCUSSION

The most significant spectral feature in all the 3-10 keV EPIC spectra of Mrk 205 and Mrk 509 is low-ionization Fe K α emission at 6.4 keV. In both sources, improved fits are obtained when an additional emission component is included, peaking at slightly higher energy; Gaussian or relativistic emission lines or cold reflection are all plausible forms for this additional spectral component. For Mrk 509, the spectral modelling requires that the 6.4 keV line is broad, FWHM > 5000 km s $^{-1}$ unless this additional component is included. More complex models, combining a second emission line with cold reflection, do not produce significantly better fits for any of the spectra than models with cold reflection but without a second emission line.

The 6.4 keV emission is a signature of reprocessing by cold material, but where does this reprocessing take place? Both galaxies show negligible intrinsic absorption in soft X-rays, and hence the material responsible for the 6.4 keV emission must lie outside the line of sight to the continuum source. Possible locations include the accretion disk, the molecular torus favoured by AGN unification schemes (Antonucci 1993), and the (optical) broad line clouds. The molecular torus and the accretion disk represent Compton thick targets, and reprocessing at these locations will result in a Compton reflection component with an edge at 7.1 keV as well as Fe K α line emission (Matt, Perola & Piro 1991, George and Fabian 1991). However, the broad line clouds are expected to be Compton thin (Shields, Ferland & Peterson 1995) and therefore the Fe K α line emission will not be accompanied by significant Compton scattered continuum.

Simulations by Leahy and Creighton (1993, see also Yaqoob et al. 2001) show that if the broad-line clouds have column densities of 10^{23} cm $^{-2}$, they would need to cover 50% of the sky, as seen by the continuum source, to produce the Fe K α line of 50 eV equivalent width in Mrk 509. To produce the 100 eV equivalent width line seen in Mrk 205, the broad line clouds would need to surround $\sim 100\%$ of the central source. These covering fractions are much higher than the typical broad line region covering fractions deduced from the ultraviolet (10% – 25%, Davidson & Netzer 1979, Goad & Koratkar 1998), suggesting that the broad line regions are probably not responsible for the majority of the Fe K α photons. Furthermore in Mrk 509, even if the broad line region does produce the Fe K α line, something else must contribute an additional broad spectral component at slightly higher energy, or else the velocity width of the Fe K α line is inconsistent with the width of the optical lines, which have FWHM of only 2270 km s $^{-1}$ (Wandel, Peterson & Malkan 1999).

On the other hand, if the Fe K α line originates in Compton thick material, the equivalent width of the line suggests that this material intercepts $\sim 30 - 60$ per cent of the emitted radiation in Mrk 205, and about half as much in Mrk 509 (George & Fabian 1991). Therefore in both AGN the strength of the Fe K α line alone suggests that a significant Compton reflection component should be present. When reflection is included in the fit we find that $> 55\%$ of the radiation is intercepted by the reflector in Mrk 205, and $> 40\%$ in Mrk 509, slightly higher than inferred from the Fe K α line but not greatly so. Thus a Compton thick reprocessor that intercepts a significant fraction of the primary X-rays can account for all the Fe K features in Mrk 205 or Mrk 509. This reprocessor could be a distant molecular torus, or the accretion disk itself. However, the velocity width of the Fe K α line implies that even if the reprocessor is the accretion disk, little of the reprocessed emission comes from the inner, relativistic, parts of the disk.

So what evidence do we have for emission from highly ionized Fe, potentially in an accretion disk? For Mrk 205, the fits with a second emission line are as good as those including a reflection component. However the second emission line is narrow when it is modeled as a Gaussian, and similarly the best fit accretion disk line is one in which the emission is dominated from material in the outer disk,

resulting in a narrow line. Hence even if the spectrum of Mrk 205 *does* include Fe XXV or Fe XXVI, there is no evidence for relativistic broadening.

For Mrk 509, the best-fit second emission line is broad, whether it is modeled as a Gaussian or as a disk line, and the steep emissivity index implies that most of the emission would come from the inner part of the disk. The disk would have an inclination of between 20 and 40 degrees, in agreement with the findings of Pounds et al. (2001). However, the χ^2/ν for the fits including an accretion disk line are only slightly better than the fits including Compton reflection for the first observation of Mrk 509, and are slightly poorer for the second observation; the combined spectrum is as well fit by either model. Hence although the features in the spectrum of Mrk 509 can be fit with a model including both a distant, cold, Compton-thin reprocessor and relativistically broadened emission from highly ionised Fe in an accretion disk, they can be fit equally well by reprocessing and Compton reflection from distant, cold material.

Thus in both Mrk 205 and Mrk 509, we find that the Fe K features can be explained by a single phase Compton thick cold reflector. While the presence of reflection from the highly ionized, high velocity, inner parts of an accretion disk is not ruled out by these data, it is not unambiguously detected.

5 CONCLUSIONS

We have analysed the 3-10 keV *XMM-Newton* EPIC spectra of Mrk 205 and Mrk 509 to investigate the Fe K features in these objects. Acceptable fits can be obtained for models containing nothing more than a power law and an emission line at 6.4 keV, consistent with cold Fe $K\alpha$. However, better fits are obtained when an additional spectral component is included in the model, either Compton reflection from cold material or an emission line from ionised Fe; the goodness of fit is similar whichever component is added. In Mrk 205, there is no evidence for relativistic broadening of any emission line, but in Mrk 509 the best fit parameters for an ionised Fe emission line suggest that it might originate in the inner regions of an accretion disk. However, illumination of distant, cold material provides a simpler, self consistent explanation of the spectral features than models including reflection from highly ionized, relativistic material. Therefore, contrary to Pounds et al. (2001) and Reeves et al. (2001b), we do not find strong evidence in either object for reprocessing in the highly ionised inner parts of an accretion disk.

6 ACKNOWLEDGMENTS

Based on observations obtained with *XMM-Newton*, an ESA science mission with instruments and contributions directly funded by ESA Member states and the USA (NASA).

REFERENCES

- Anders E., & Grevesse N., *Geochimica et Cosmochimica Acta*, 1989, 53, 197
- Antonucci R., 1993, *Annu. Rev. Astron. Astrophys.*, 31, 473
- Blustin A.J., Branduardi-Raymont G., Behar E., Kaastra J.S., Kahn S.M., Page M.J., Sako M., Steenbrugge K.C., 2002, *A&A*, in press
- Davidson K., & Netzer H., 1979, *Rev. Mod. Phys.*, 51, 715
- Dickey J.M., & Lockman F.J., 1990, *Annu. Rev. Astron. Astrophys.*, 28, 215
- Fabian A.C., Rees M.J., Stella L., White N.E., 1989, *MNRAS*, 238, 729
- George I.M., Fabian A.C., 1991, *MNRAS*, 249, 352
- Goad K., & Koratkar A., 1998, *ApJ*, 495, 718
- Leahy D.A., & Creighton J., 1993, *MNRAS*, 263, 314
- Magdziarz P., & Zdziarski A.A., 1995, *MNRAS*, 273, 837
- Matt G., Perola G.C., & Piro L., 1991, *A&A*, 247, 25
- Nandra K., George I.M., Mushotzky R.F., Turner T.J., Yaqoob T., 1997, *ApJ*, 477, 602
- Pounds K., Reeves J., O'Brien P., Page K., Turner M., Nayakshin S., 2001, *ApJ*, 559, 181
- Reeves J.N., Turner M.J.L., Bennie P.J., Pounds K.A., Short A., O'Brien P.T., Boller Th., Kuster M., Tiengo A., 2001, *A&A*, 365, L116
- Reeves J.N., Turner M.J.L., Pounds K.A., O'Brien P.T., Boller Th., Ferrando P., Kendziorra E., Vercellone S., 2001, *A&A*, 365, L134
- Reynolds C.S., 1997, *MNRAS*, 286, 513
- Shields J.C., Ferland G.J., Peterson B.M., 1995, *ApJ*, 441, 507
- Tanaka Y., Nandra K., Fabian A.C., Inoue H., Otani C., Dotani T., Hayashida K., Iwasawa K., Kii T., Kunieda H., Makino F., Matsuoka M., 1995, *Nature*, 375, 659
- Wandel A., Peterson B.M., & Malkan, M.A., 1999, *ApJ*, 526, 579
- Yaqoob T., George I.M., Nandra K., Turner T.J., Serlemitsos P.J., Mushotzky R.F., 2001, *ApJ*, 546, 759

APPENDIX A: METHOD TO COMBINE SPECTRA FROM EPIC MOS AND EPIC PN CAMERAS

The following method was designed with pulse height spectra and response matrices in standard ‘OGIP’¹ format in mind. We use the term ‘response matrix’ to refer to the product of the effective area and the energy→channel redistribution matrix.

We wish to combine a number of individual source+background pulse-height spectra to a single pulse-height spectrum. We label each individual spectrum with the index $s = 1, 2, \dots, N_{spec}$, and we use the index $i = 1, 2, \dots, N_{chan}(s)$ to denote the channels of each spectrum. Each channel is assigned a ‘nominal’ energy range of $ENOM_{min}(i) < E < ENOM_{max}(i)$. The number of photons in each channel i of spectrum s is $C(s, i)$. In general, each source+background spectrum $C(s, i)$ has a corresponding background spectrum $B(s, i)$, with a scaling factor $F(s)$ relating the geometric area and/or exposure times of the two spectra. Each of the original spectra has a corresponding response matrix, whose elements contain

¹ http://heasarc.gsfc.nasa.gov/docs/heasarc/ofwg/docs/spectra/ogip_92_007/ogip_92_007.html

the effective area for a given channel and a given energy range. The element of the response matrix for spectrum s corresponding to a particular channel i and a particular energy range $E_{min}(j) < E < E_{max}(j)$ (where $j = 1, 2, \dots, N_{range}(s)$) is denoted $R(s, i, j)$. Throughout we use capitalised indices when referring to the summed spectrum and response matrix; the index s is omitted when referring to a combined spectrum or response matrix.

We define the fractional overlap of channel i of spectrum s with channel I of the combined spectrum to be if $ENOM_{min}(s, i) < ENOM_{max}(I)$

and $ENOM_{max}(s, i) > ENOM_{min}(I)$

$$f(s, i, I) = \frac{\{ \min[ENOM_{max}(s, i), ENOM_{max}(I)] - \max[ENOM_{min}(s, i), ENOM_{min}(I)] \}}{\{ ENOM_{max}(s, i) - ENOM_{min}(s, i) \}}$$

otherwise

$$f(s, i, I) = 0 \quad (\text{A1})$$

The combined spectrum is constructed by summing all the counts from all the spectra in the nominal energy range of each channel. So,

$$C(I) = \sum_{s=1}^{N_{spec}} \sum_{i=1}^{N_{chan}(s)} f(s, i, I) C(s, i) \quad (\text{A2})$$

If the nominal energy ranges of the channels of the different spectra do not coincide with those of the combined spectrum, some randomization of photons will be required to ensure that the channels of the output spectrum contain integer numbers of counts.

We combine the individual background spectra into a single background spectrum with a single scaling factor F . The following scheme produces a background photon spectrum with the signal to noise ratio propagated from the individual background spectra.

$$B(I) = \frac{1}{F} \sum_{s=1}^{N_{spec}} F(s) \sum_{i=1}^{N_{chan}(s)} B(s, i) \quad (\text{A3})$$

where

$$F = \frac{\sum_{s=1}^{N_{spec}} F^2(s) \sum_{i=1}^{N_{chan}(s)} B(s, i)}{\sum_{s=1}^{N_{spec}} F(s) \sum_{i=1}^{N_{chan}(s)} B(s, i)} \quad (\text{A4})$$

The response matrices are easily combined without any complicated weighting, provided that the pulse height spectra are all realisations of a single spectrum (e.g. if they are from observations of the same source at the same time but by different instruments). If the individual pulse height spectra are realisations of *intrinsically different* spectra, then the response matrix combination described here will not generally be appropriate. However if the spectra differ only in intensity then a simple scaling factor can be used to weight the contributions of the different response matrices to the final spectrum. For each energy range of the combined response matrix, the elements corresponding to each channel are combined in the same way as the original spectra. This is more complicated if the energy ranges differ between the response matrices. In this case we use a weighted average response for a given energy range. We define the fractional overlap of energy range j of spectrum s with the energy range J of the output response matrix as follows:

if $E_{min}(s, j) < E_{max}(J)$

and $E_{max}(s, j) > E_{min}(J)$

$$g(s, j, J) = \frac{\min[E_{max}(s, j), E_{max}(J)] - \max[E_{min}(s, j), E_{min}(J)]}{E_{max}(s, j) - E_{min}(s, j)}$$

otherwise

$$g(s, j, J) = 0 \quad (\text{A5})$$

The combined response matrix is then constructed according to:

$$R(I, J) = \sum_{s=1}^{N_{spec}} \sum_{i=1}^{N_{chan}(s)} f(s, i, I) \frac{\sum_{j=1}^{N_{range}(s)} g(s, j, J) R(s, i, j)}{\sum_{j=1}^{N_{range}(s)} g(s, j, J)} \quad (\text{A6})$$